JCI The Journal of Clinical Investigation

Anti-EGFL7 antibodies enhance stress-induced endothelial cell death and anti-VEGF efficacy

Leisa Johnson, … , Weilan Ye, Priti S. Hegde

J Clin Invest. 2013;123(9):3997-4009. https://doi.org/10.1172/JCI67892.

Research Article **Oncology**

Many oncology drugs are administered at their maximally tolerated dose without the knowledge of their optimal efficacious dose range. In this study, we describe a multifaceted approach that integrated preclinical and clinical data to identify the optimal dose for an antiangiogenesis agent, anti-EGFL7. EGFL7 is an extracellular matrix–associated protein expressed in activated endothelium. Recombinant EGFL7 protein supported EC adhesion and protected ECs from stress-induced apoptosis. Anti-EGFL7 antibodies inhibited both of these key processes and augmented anti-VEGF–mediated vascular damage in various murine tumor models. In a genetically engineered mouse model of advanced non–small cell lung cancer, we found that anti-EGFL7 enhanced both the progression-free and overall survival benefits derived from anti-VEGF therapy in a dose-dependent manner. In addition, we identified a circulating progenitor cell type that was regulated by EGFL7 and evaluated the response of these cells to anti-EGFL7 treatment in both tumor-bearing mice and cancer patients from a phase I clinical trial. Importantly, these preclinical efficacy and clinical biomarker results enabled rational selection of the anti-EGFL7 dose currently being tested in phase II clinical trials.

Anti-EGFL7 antibodies enhance stress-induced endothelial cell death and anti-VEGF efficacy

Leisa Johnson,[1] Mahrukh Huseni,[1] Tanya Smyczek,[1] Anthony Lima,[1] Stacey Yeung,[1] Jason H. Cheng,[1] Rafael Molina,[1] David Kan,[1] Ann De Mazière,[2] Judith Klumperman,[2] Ian Kasman,[1] Yin Zhang,[1] Mark S. Dennis,[1] Jeffrey Eastham-Anderson,[1] Adrian M. Jubb,[1] Olivia Hwang,[1] Rupal Desai,[1] Maike Schmidt,[1] Michelle A. Nannini,[1] Kai H. Barck,[1] Richard A.D. Carano,[1] William F. Forrest,[1] Qinghua Song,[1] Daniel S. Chen,[1] Louie Naumovski,[1] Mallika Singh,[1] Weilan Ye,[1] and Priti S. Hegde[1]

[1]Genentech Inc., South San Francisco, California, USA. [2]Cell Microscopy Center, Department of Cell Biology, University Medical Center Utrecht and Institute for Biomembranes, Utrecht, the Netherlands.

Many oncology drugs are administered at their maximally tolerated dose without the knowledge of their optimal efficacious dose range. In this study, we describe a multifaceted approach that integrated preclinical and clinical data to identify the optimal dose for an antiangiogenesis agent, anti-EGFL7. EGFL7 is an extracellular matrix–associated protein expressed in activated endothelium. Recombinant EGFL7 protein supported EC adhesion and protected ECs from stress-induced apoptosis. Anti-EGFL7 antibodies inhibited both of these key processes and augmented anti-VEGF–mediated vascular damage in various murine tumor models. In a genetically engineered mouse model of advanced non–small cell lung cancer, we found that anti-EGFL7 enhanced both the progression-free and overall survival benefits derived from anti-VEGF therapy in a dose-dependent manner. In addition, we identified a circulating progenitor cell type that was regulated by EGFL7 and evaluated the response of these cells to anti-EGFL7 treatment in both tumor-bearing mice and cancer patients from a phase I clinical trial. Importantly, these preclinical efficacy and clinical biomarker results enabled rational selection of the anti-EGFL7 dose currently being tested in phase II clinical trials.

Introduction

Antiangiogenesis (AA) is an important and effective therapeutic modality in the treatment of multiple solid tumors. The most broadly used AA agent is Avastin (hereafter referred to as bevacizumab), a monoclonal antibody that blocks the activity of VEGF (1). Although VEGF has many cellular functions, its EC survival activity is believed to be the major factor contributing to anti-VEGF–mediated efficacy (2), as vascular loss is a prominent feature found in tumors that have been deprived of VEGF signaling (3–6). To augment the activity of anti-VEGF, we searched for factors that provide survival support to ECs, particularly under nutrient- and oxygen-deprived conditions, as these stresses mimic key microenvironmental features following VEGF inhibition. We identified an ECM-associated protein, epidermal growth factor–like 7 (EGFL7), which meets these criteria.

EGFL7 is a secreted protein produced by nascent tumor blood vessels as well as vessels in other proliferating tissues, but it is absent or expressed at low levels in healthy quiescent vessels as well as many nonvascular cell types (7–11). Upon secretion, EGFL7 becomes tightly associated with the perivascular extracellular matrix and supports EC adhesion and migration (10, 12). In addition, EGFL7 protects ECs from hyperoxic stress–induced apoptosis (13). Furthermore, the loss or gain of *Egfl7* expression results in aberrant vascular development (10, 14).

In this study, we demonstrate that recombinant EGFL7 protein protects ECs under multiple stress conditions. Antibodies against anti-EGFL7 block the adhesive and prosurvival activities of EGFL7 in vitro. In addition, we show that in vivo administration of anti-EGFL7 antibodies enhanced both the AA activity and survival benefits resulting from VEGF blockade in human xenograft tumor models as well as genetically engineered mouse models (GEMMs) of cancer (15).

Recently, new clinical evidence demonstrated that prolonged administration of bevacizumab alone provided substantially greater progression-free survival (PFS) benefit relative to short-term use of bevacizumab in combination with chemotherapy (16), highlighting the importance of sustained inhibition of tumor angiogenesis. Given the potential of long-term use of antiangiogenic agents in the clinic, it is desirable to identify biologically active doses that are well tolerated. These considerations emphasize the need for optimization of clinical dose and duration of treatment for AA agents. Historically, dose selection for drugs in oncology has relied on identification of a

Authorship note: Leisa Johnson, Mahrukh Huseni, Tanya Smyczek, and Anthony Lima contributed equally to this work.

Conflict of interest: The following authors are or were employees of Genentech Inc., a member of the Roche Group, and hold or held equity in Genentech/Roche during the course of this work: L. Johnson, M. Huseni, T. Smyczek, A. Lima, S. Yeung, J.H. Cheng, R. Molina, D. Kan, I. Kasman, Y. Zhang, M.S. Dennis, J. Eastham-Anderson., A.M. Jubb, O. Hwang, R. Desai, M. Schmidt, M.A. Nannini, K.H. Barck, R.A.D. Carano, W.F. Forrest, Q. Song, D.S. Chen, L. Naumovski, M. Singh, W. Ye, and P.S. Hegde. The following authors are no longer at Genentech/Roche and are currently employed by and hold equity in the following companies: L. Naumovski (AbbVie) and M. Singh (Novartis). The following authors are no longer at Genentech/Roche: I. Kasman and O. Hwang. The following authors receive research support from Genentech/Roche: A. De Mazière and J. Klumperman. Genentech/Roche owns all patent rights.

Citation for this article: *J Clin Invest.* 2013;123(9):3997–4009. doi:10.1172/JCI67892.

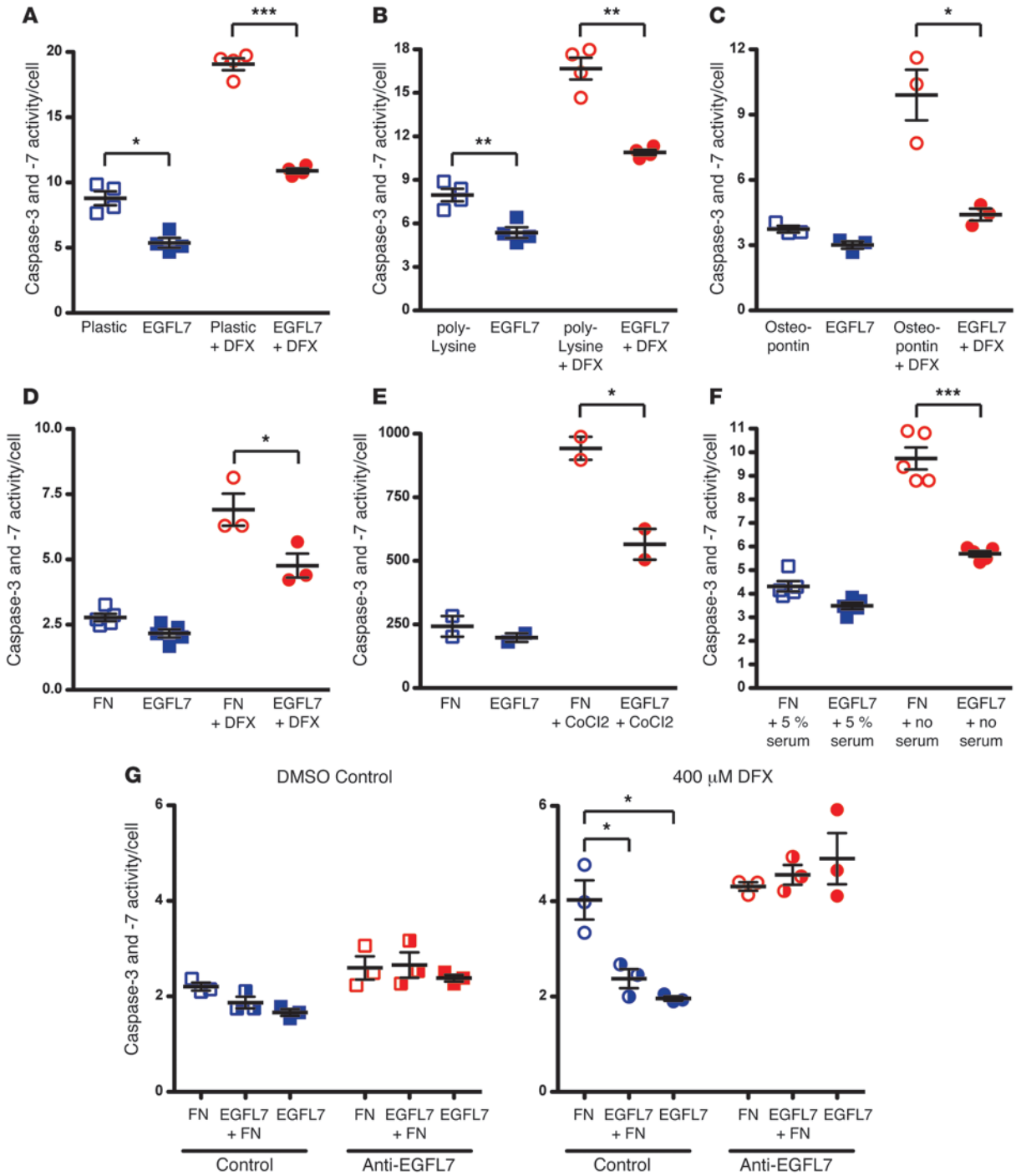

Figure 1

Recombinant EGFL7 protein decreases stress-induced EC apoptosis. Cleaved caspase-3 and caspase-7 (*y* axis) activity were measured on HUVECs cultured for 16 hours under the conditions indicated on the *x* axis. Higher values on the *y* axis indicate increased EC death. In all panels, filled symbols represent data derived from HUVECs cultured on tissue culture plates coated with EGFL7 protein, whereas open symbols represent data from HUVECs cultured on plates coated with other substances, including culture medium (**A**), poly-lysine (**B**), osteopontin (**C**), and fibronectin (FN) (**D**–**F**). Cells were cultured in serum-containing medium with DMSO as the negative control (blue symbols, **A**–**F**) or treated with the hypoxic mimetics DFX at 400 μM (red symbols, **A**–**D**) or $CoCl_2$ at 200 μM (red symbols, **E**), or cultured in serum-free medium (red symbols, **F**), and then assayed for cleaved caspase-3 and caspase-7 normalized to cell counts, where feasible (**A**–**D** and **F**; see Methods). HUVEC apoptosis assay was also carried out as described above in the presence of a control antibody or the humanized anti-EGFL7 antibody, h18F7 (**G**). While EGFL7 or a mixture of EGFL7 with fibronectin reduced DFX-induced apoptosis, anti-EGFL7 abolished the activity of the EGFL7 protein. Each symbol represents 2 to 5 independent measurements; the mean ± the SEM is depicted. *P* values were calculated by unpaired, 2-tailed Student's *t* test. $^{*}P < 0.05$; $^{**}P < 0.005$; $^{***}P < 0.0005$.

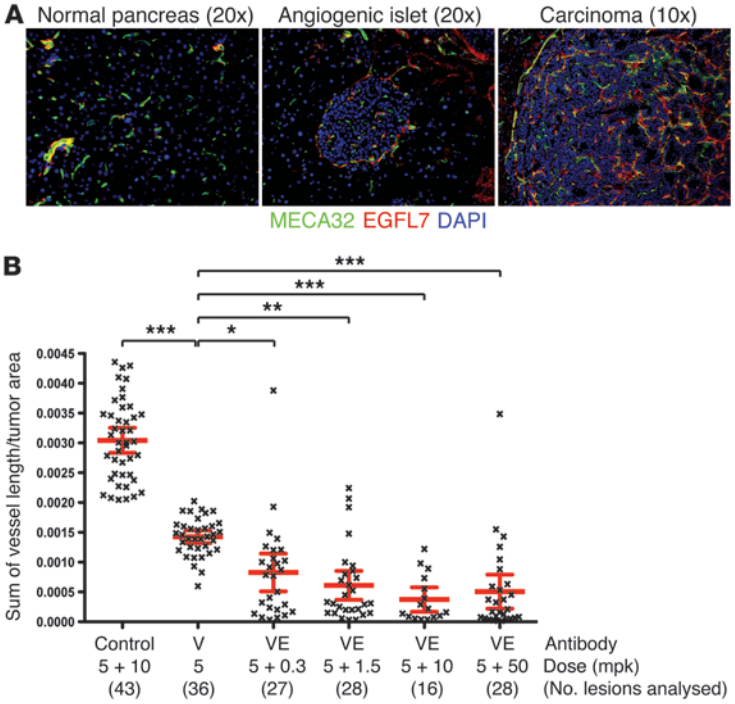

Figure 2
Anti-EGFL7 enhances the activity of anti-VEGF in the *RIP-TβAg* insulinoma model. (**A**) Representative IF-stained photomicrographs of EGFL7 (red) and the vascular EC membrane marker MECA32 (green) expression in wild-type mouse pancreas (left panel) and in angiogenic islets (middle panel) and invasive carcinomas (right panel) from *RIP-TβAg* transgenic mice. EGFL7 is present in the perivascular matrix of a subset of blood vessels in normal pancreata and angiogenic islets and in the majority of tumor vessels. (**B**) Quantitative analysis of microvascular densities in invasive carcinomas after 2 weeks of treatment with IgG2a control anti-ragweed antibody, anti-VEGF (V) (B20-4.1.1), anti-EGFL7 (E) (h18F7), or the combination (VE). All antibodies were dosed via i.p. injection 1 time per week on days 1 and 8. The total number of individual lesions analyzed is indicated below each cohort and originated from 3–5 animals per group, with 1 to 16 tumors per animal. Each dot represents vascular area/tumor area, with mean values ± 95% CI shown. *P* values were calculated using a mixed-effects model, with the anti-VEGF group serving as the comparator for all other cohorts. $^{*}P < 0.05$; $^{**}P < 0.005$; $^{***}P < 0.0005$. Please see the Supplemental Methods for additional details. Please note that some or all of the mice from the C, V, and VE (E at 1.5 and 10 mpk) cohorts were used to used to generate additional data presented in Figure 7F and Supplemental Figure 7E.

maximum tolerated dose (MTD) or economically feasible dose (17). Monoclonal antibodies are targeted therapies with specific mechanisms of action and are generally better tolerated than cytotoxic agents; therefore many targeted agents have relatively broad therapeutic windows. Thus, identification of a biologically active dose becomes an important factor for the clinical development of drug candidates. Incorporation of biomarkers with adequate preclinical justification for evaluation in clinical trials is now increasingly being used to allow for rational dose selection in larger efficacy studies. We identified a population of circulating progenitor cells (CPCs) to serve as a pharmacodynamic (PD) marker for interrogating the in vivo activities of anti-EGFL7 in mice and humans. By evaluating the antitumor activity in GEMMs and PD biomarkers in phase I patients, we selected an efficacious dose of anti-EGFL7 that is below the MTD for further clinical evaluation. Our study suggests that anti-EGFL7 could be an efficacious therapeutic agent for the treatment of solid cancers, and we demonstrate the power of integrating preclinical and clinical studies to inform dose selection in later-stage clinical trials.

Results

EGFL7 plays an important prosurvival role for ECs under stress. Systemic inhibition of VEGF activity prunes back the tumor vasculature, resulting in a tumor microenvironment low in vital nutrients and oxygen. We hypothesized that targeting mechanisms that protect ECs from stress-induced cell death could augment the activity and efficacy achieved with anti-VEGF. To test this hypothesis, we conducted a small-scale screen for factors that provide survival support to primary HUVECs under nutrient- or oxygen-deprivation stresses. We evaluated a number of secreted factors, including ECM proteins, and found that recombinant EGFL7 protein played a marked role in protecting ECs from stress-induced death. Using cleaved caspases 3 and 7 as indicators of apoptosis, we found that EGFL7-coated plates significantly enhanced the survival of HUVECs exposed to low oxygen, hypoxic mimics, or low nutrients compared with cells grown on several other ECM substrates or artificially treated surfaces (Figure 1, A–F, and data not shown). The activity of these hypoxic mimetics was confirmed by their ability to increase HIF1α protein (Supplemental Figure 1A; supplemental material available online with this article; doi:10.1172/JCI67892DS1) and the downstream expression of classical HIF1α target genes (Supplemental Figure 1B). Interestingly, under nutrient rich and normoxic conditions, EGFL7 did not always recognizably differ from other ECM substrates, indicating that the prosurvival activity of EGFL7 is more prominent under conditions of stress.

The in vitro activity of EGFL7 reported above led us to hypothesize that blocking EGFL7 function could enhance the ability of anti-VEGF to damage tumor vessels, thereby increasing the antitumor efficacy achieved with anti-VEGF. To test this hypothesis, we developed a panel of anti-EGFL7 antibodies as previously reported (10). To identify antibodies that could be tested preclinically in mouse models of cancer, we screened for antibodies that bound to human and mouse EGFL7 with comparable affinities and that also inhibited the adhesive and prosurvival activity of EGFL7 as determined using an in vitro cell–based assay. Two antibodies (designated as 18F7 and 10G9) that met all binding affinity and in vitro activity criteria (Figure 1G and Supplemental Figure 2) were chosen to carry out further studies described hereafter. Using a process called humanization, one of the antibodies (18F7) was reformatted into the human IgG1 backbone to enable eventual testing in cancer patients, and we confirmed that the binding affinity and in vitro activities of 18F7 were preserved after humanization (Supplemental Figure 3).

Anti-EGFL7 enhances anti-VEGF activity as assessed by tumor microvascular density in the RIP-TβAg GEMM. The in vitro activities of EGFL7 protein and its antibodies predict that anti-EGFL7 may enhance

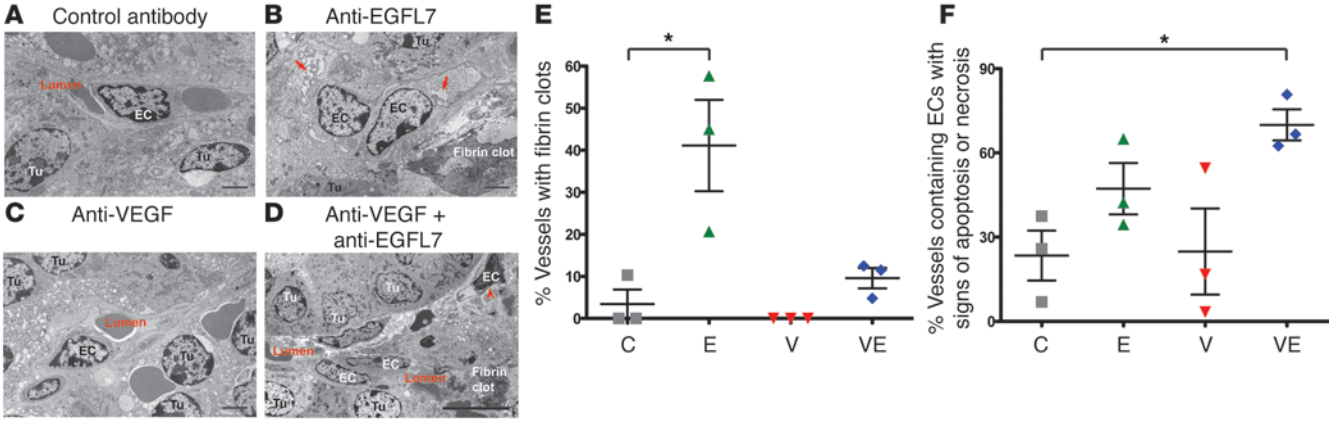

Figure 3

TEM analysis of tumor vessels in the *RIP-TβAg* insulinomas. (**A**–**D**) Representative images of invasive carcinomas from *RIP-TβAg* mice treated with antibodies indicated on top of each panel. Anti-EGFL7 (m18F7) was administered at 1 mpk and anti-VEGF (B20-4.1.1) at 5 mpk; both were dosed i.p., 1 time per week. Tissues were analyzed 14 days after treatment initiation. Blood vessels in the anti-EGFL7–treated groups were often associated with fibrin clots, and many ECs showed damage in the form of distension of the RER cisterns (arrows in **B**) and/or the nuclear envelope, which are signs of necrosis. In all treatment groups, some ECs showed early signs of apoptosis including unusually condensed cytoplasm and nucleoplasm (arrowhead in **D**). ECs with evidence of apoptosis and/or necrosis were more frequently found in the combination treatment group than the control group. Tu, tumor cell; lumen, vessel lumen. Scale bars: 2 μm (**A**–**C**), 10 μm (**D**). (**E**) Fibrin clot–associated vessels were counted and normalized to total vessels. C, control. (**F**) Vessels containing ECs with evidence of apoptosis or necrosis were counted and normalized to total vessels. Dots in **E** and **F** represent individual tumors; 1–2 tumors/animal and 2–3 animals/group were analyzed. If multiple fields of view were analyzed from a single tumor, the mean value was calculated to represent the designated tumor. The mean ± SEM is depicted. *P* values were calculated by unpaired, 2-tailed Student's *t* test. *$P < 0.05$.

the AA effect of VEGF blockade. Because anti-VEGF therapy is used to treat multiple, diverse types of cancer in the clinic, we utilized a variety of preclinical tumor models to test this hypothesis. We chose models that are noticeably, but not completely, inhibited by anti-VEGF treatment in order to demonstrate improvement of anti-VEGF efficacy in several different settings. Furthermore, since anti-VEGF activity appears to be independent of tumor cell genotypes (18), we chose models with differing oncogenic drivers to evaluate whether this new therapy could be broadly applicable. Finally, since our goal was to demonstrate mechanism-driven enhancement of anti-VEGF activity, we administered anti-VEGF at an individually tailored dose and schedule that was predetermined to induce maximal tumor growth inhibition in each model.

First, we wanted to determine whether anti-EGFL7 could enhance the antitumor angiogenesis activity of anti-VEGF. To this end, we utilized a transgenic model of insulinoma driven by ectopic expression of large-T antigen in the β cells of pancreatic islets, termed *RIP-TβAg* (19). We chose this model because of its well-established angiogenesis attributes and narrow distribution of vascular densities. Importantly, the vascular response to anti-VEGF is homogeneous across individual tumors, thereby enabling a more robust evaluation of tumor microvascular density (MVD) changes relative to other models (20, 21). We first established that EGFL7 is abundantly expressed in tumor vessels in this model (Figure 2A). We then treated *RIP-TβAg* transgenic tumor-bearing mice at the age of 11–12 weeks with control antibody, anti-VEGF (B20-4.1.1) (15), or anti-VEGF in combination with the humanized anti-EGFL7 18F7 (h18F7) at a range of concentrations. After 14 days on treatment, pancreases were harvested and insulinomas characterized for their MVD via immunohistochemistry. Multiple invasive carcinomas from each animal were analyzed for vascular density. Anti-VEGF antibody alone significantly reduced MVD, and combination with anti-EGFL7 (h18F7) further decreased MVD (Figure 2B), indicating that blocking EGFL7 function does indeed enhance the effect of VEGF inhibition. The activity of anti-EGFL7 (h18F7) was evident at the lowest tested dose, although higher doses trended toward further reduction of MVD (Figure 2B). The differences between all tested doses were not significant. In separate studies, we found that anti-EGFL7 (h18F7) treatment alone did not consistently and significantly reduce tumor MVD in this model (data not shown), indicating that the combination activity reflects the ability of anti-EGFL7 to enhance the efficacy of anti-VEGF.

The in vivo data described above suggest that anti-EGFL7 and anti-VEGF may function together effectively to cause tumor vessel damage. We sought to evaluate tumor EC apoptosis using conventional histology methods, including TUNEL, H2AX, and cleaved caspase staining, but were unable to detect significant numbers of apoptotic ECs even in tumors with appreciable MVD reduction, presumably due to rapid removal of apoptotic ECs from the endothelium. To overcome this technical hurdle, we utilized transmission electron microscopy (TEM) to carefully examine tumor vessels in the *RIP-TβAg* insulinomas treated with control antibody, anti-EGFL7 (h18F7), anti-VEGF, or the combination. We found that tumor vessels treated with anti-EGFL7 (h18F7) were frequently associated with fibrin clots (Figure 3, B and E), possibly indicating subphenotypic damage that was not sufficient to cause MVD reduction. In some tumors, EC damage was evident as indicated by distension of rough endoplasmic reticulum (RER) cisterns and/or the nuclear envelope (Figure 3, B and F), which may represent evidence of necrosis. In addition, we observed ECs with early signs of apoptosis — exceptionally dense nucleoplasm and cytoplasm (Figure 3, D and F). The frequency of blood vessels containing ECs with evidence of apoptosis or necrosis was significantly higher in the combination treatment group than in the control group and

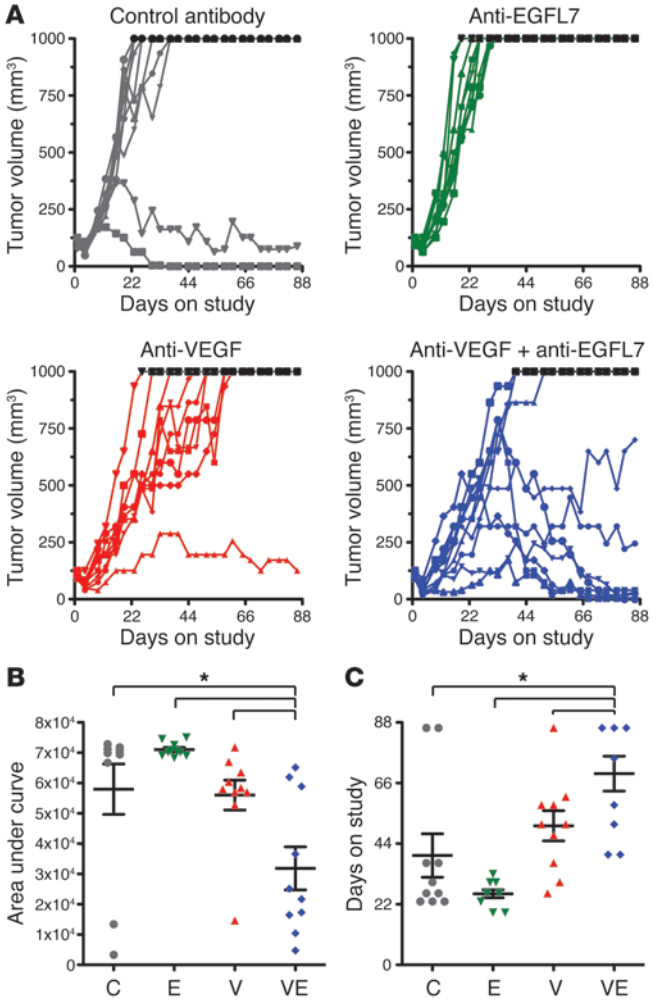

Figure 4
Combination of anti-EGFL7 plus anti-VEGF inhibits the growth of xenografted H1299 NSCLC tumors. (**A**) Four groups of mice (10 each) were treated with the indicated antibodies. Individual tumor growth curves from mice harboring established tumors and dosed i.p. with control anti-ragweed (10 mpk, 1 time per week), anti-EGFL7 m18F7 (10 mpk, 2 times per week), anti-VEGF B20-4.1 (10 mpk, 1 time per week), or the combination of m18F7 plus B20-4.1. All treatments were dosed until tumors reached 1000 mm^3, and the study was terminated on day 86. Tumors that reached end point before day 86 were continuously plotted at the end point volume of 1000 mm^3 (black dots at the top). (**B**) Due to variable growth patterns, tumor growth was compared across treatments using an AUC measurement between days 0 and 86. Smaller AUC values represent slower growth. Tumors treated with combination therapy grew significantly more slowly than tumors in all other treatment cohorts, whereas tumors treated with either anti-EGFL7 or anti-VEGF monotherapy grew at a rate comparable to that of control. (**C**) The number of days each animal stayed on the study is another parameter reflecting tumor growth rates, as animals were taken off the study when their tumors reached 1000 mm^3. Animals treated with the combination therapy stayed on study significantly longer than all other groups. The mean ± SEM is depicted. *P* values were calculated by unpaired, 2-tailed Student's *t* test. $^*P < 0.05$.

trended toward being higher than the anti-VEGF–treated group ($P = 0.0505$), supporting our hypothesis that anti-EGFL7 and anti-VEGF function together to cause damage to tumor endothelium.

Combination of anti-EGFL7 and anti-VEGF inhibits tumor growth in a non–small cell lung cancer xenograft model. The AA activity described above suggests that the combination of anti-EGFL7 and anti-VEGF may suppress tumor growth. To test this hypothesis, we treated mice harboring established xenografted tumors derived from the non–small cell lung cancer (NSCLC) cell line H1299 with control antibody, anti-VEGF (B20-4.1), anti-EGFL7 (murine 18F7, m18F7), or the combination of anti-VEGF and anti-EGFL7. While single-agent anti-VEGF and anti-EGFL7 did not significantly alter growth of the xenografted H1299 tumors, the combination of both agents resulted in significant tumor growth suppression (Figure 4, A and B) and prolongation of time on study (Figure 4C), indicating that anti-EGFL7 and anti-VEGF can function together to suppress tumor growth. Interestingly, a dose escalation study in this same model failed to differentiate among the doses examined, with combination antitumor activity saturating at the lowest anti-EGFL7 dose (0.2 mg/kg [mpk]) tested (Supplemental Figure 4).

Anti-EGFL7 augments the activity of anti-VEGF in a dose- and duration-dependent manner in an NSCLC GEMM. We next examined the efficacy of anti-EGFL7 in combination with anti-VEGF in an autochthonous model of NSCLC, an indication for which bevacizumab is currently approved. We have previously validated and preclinically assessed a mutant $Kras^{G12D};p53^{Frt/Frt}$-driven GEMM of NSCLC (15). Given the significant short- and long-term efficacy that we observed with anti-VEGF (B20-4.1.1) (15, 21), we believed this model was ideally suited for testing the effects of anti-EGFL7 in combination with anti-VEGF in epithelial carcinomas. In addition, we found that EGFL7 expression is initially upregulated in early-stage atypical adenomatous hyperplasia (AAH), and remains upregulated in the tumor vasculature of both benign adenomas (Ad), and malignant adenocarcinomas (AdC) (Figure 5A) in this model.

Given the dose-response pattern observed in the *RIP-TβAg* model, we chose to examine a wide range of anti-EGFL7 (m18F7) doses in combination with the maximally efficacious dose regimen of anti-VEGF (B20-4.1.1) as determined previously (data not shown). $Kras^{G12D};p53^{Frt/Frt}$ tumor-bearing mice were treated long term starting at 16 weeks post induction (wpi) with control antibody, anti-VEGF, or anti-VEGF in combination with m18F7. Serial in vivo micro-CT (micro-CT) imaging was performed to monitor tumor growth rates over time and determine response rates as well as PFS. The combination of anti-VEGF with m18F7 at 1.0 mpk provided the most durable response as evaluated by the combined number of partial responses (PRs) and stable disease (StD) (see Methods) out to 6 weeks after the start of the study (Table 1 and Supplemental Figure 5). This provided a significant increase in both PFS ($P = 0.0147$; HR = 0.56, $P = 0.0412$) and overall survival (OS) ($P = 0.0152$; HR = 0.51, $P = 0.0078$) relative to anti-VEGF monotherapy (Figure 5, D and E).

We next wanted to assess whether short-term combination therapy was equivalent to continuous treatment as measured by these same study end points. Continuous anti-VEGF plus m18F7 (1.0 mpk) treatment provided significantly improved response rates ($P = 3.91 \times 10^{-5}$), PFS ($P = 0.0011$; HR = 0.28, $P = 8.08 \times 10^{-6}$), and OS ($P = 0.0003$; HR = 0.28, $P = 8.74 \times 10^{-6}$) relative to treatment that was discontinued after 2 weeks (Table 2, Figure 6, and Supplemental Figure 6).

CPCs are a circulating biomarker of anti-EGFL7 activity. These efficacy studies underscore the importance of selecting the right

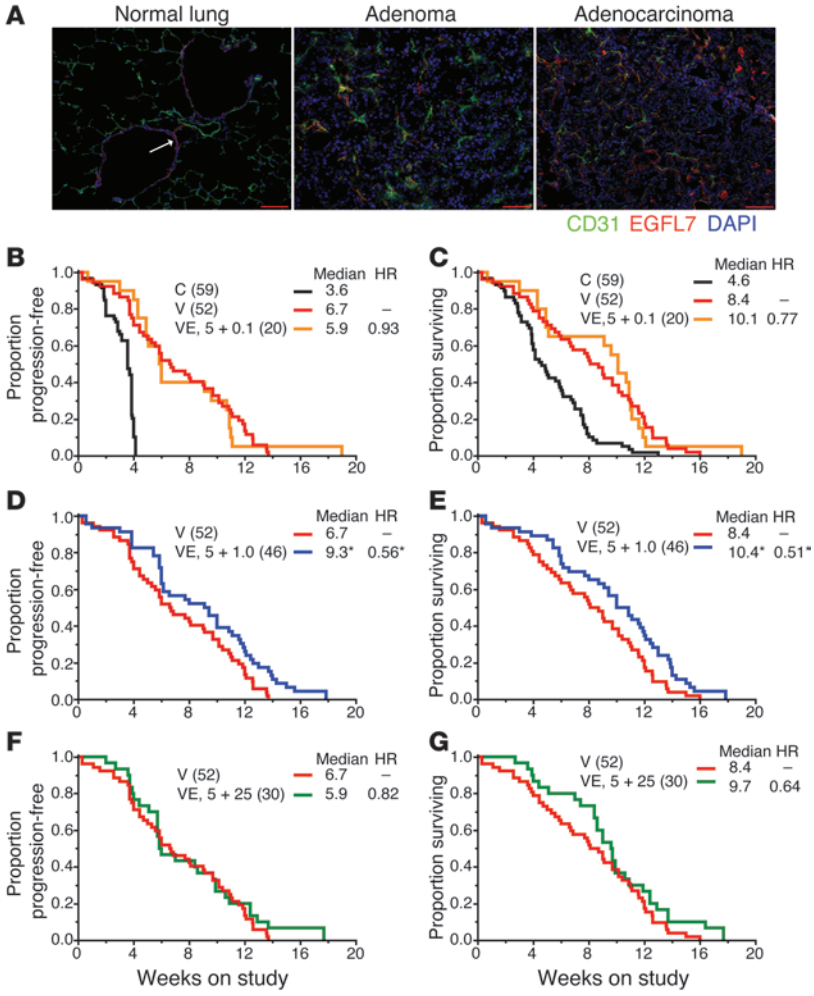

Figure 5

Anti-EGFL7 significantly improves the benefit provided by anti-VEGF in a dose-dependent manner in the *Kras*^{G12D};*p53*$^{Frt/Frt}$ NSCLC GEMM. (**A**) Representative IF-stained photomicrographs of EGFL7 (red) and CD31 (green) expression in normal mouse lung (left panel), Ads (middle panel). and invasive AdCs (right panel) from *Kras*^{G12D};*p53*$^{Frt/Frt}$ mice. EGFL7 is present in bronchial airways and the perivascular matrix of lymphatic vessels (white arrow) in normal lung, as well as the perivascular matrix of the majority of benign and malignant tumor vessels. Scale bars: 100 μm. (**B**–**G**) Kaplan-Meier plots depicting PFS (**B**, **D**, and **F**) and OS (**C**, **E**, and **G**) rates following long-term therapeutic inhibition. The number of mice/cohort is listed in parentheses. Median survival (in weeks) and HR relative to V are shown. Only the VE (5 + 1.0 mpk) combination treatment cohort provided significantly improved PFS and OS benefits relative to V (*$P < 0.05$), as determined by both log-rank and Cox-proportional hazard analyses. For panels **B**–**G**, mice were dosed i.p. 2 times per week with control anti-ragweed IgG2a (5 mpk + 1.0 mpk), anti-VEGF (B20-4.1.1; 5 mpk), or the combination of anti-VEGF (5 mpk) plus anti-EGFL7 (m18F7) at 0.1 mpk (**B** and **C**), 1.0 mpk (**D** and **E**), or 25 mpk (**F** and **G**). The same V cohort is reproduced across similar types of plots. Note: OS curves for the C and V treatment cohorts in panels **C**, **E**, and **G** are reproduced with permission from the *Journal of Pathology* (21).

dose for evaluating clinical efficacy. Therefore, we searched for a PD marker that would allow us to assess drug activity in cancer patients. Gene expression profiling of RNA from peripheral blood cells identified CD34$^+$ cells as particularly high expressers of *Egfl7* transcript (Supplemental Figure 7A). PBMCs derived from patients with acute myeloid leukemia exhibited the highest levels of *Egfl7* transcript, presumably due to the high prevalence of peripheral CD34$^+$ cells in this tumor type. To further characterize the CD34$^+$ cells expressing *Egfl7*, FACS studies were conducted in peripheral blood from healthy donors. In circulation, CD34$^+$ cells exist as 2 distinct populations: CD34^{hi}CD31^{dim}CD45^{dim} cells or CD34$^+$CD31$^+$CD45^{dim} cells (Figure 7A). These cell populations were sorted from healthy donor PBMCs, and *Egfl7* transcript expression was evaluated by quantitative RT-PCR (qRT-PCR). *Egfl7* transcripts were predominantly expressed in the CD34^{hi}CD31^{dim} CD45^{dim} cell type (Figure 7B). These cells also expressed markers of progenitor cells, including CD133, CD117 and *Aldha1* (Supplemental Figure 7B); hence, we termed these cells CPCs. The second population of CD34$^+$CD31$^+$CD45^{dim} cells expressed *Vegf* as well as classical markers of ECs including *Vegf* receptors, *vWF*, and *Itgb3* among others (Supplemental Figure 7B), hence we classified these as circulating ECs (CECs).

To determine whether CPCs have the ability to differentiate into ECs, we purified these cells from healthy donor PBMCs and cultured them in Endocult Medium (StemCell Technologies) on fibronectin-coated tissue culture plates. After 7–21 days in culture, immunofluorescence staining and FACS analyses were performed to evaluate surface expression of EC markers. Expression of EC markers including VEGFR2, CD105, and CD31 was observed in a distinct population of differentiated cells (Figure 7C and Supplemental Figure 7C). Importantly, expression of these markers was not detected in freshly isolated CPCs (data not shown), indicating that CPCs can differentiate into ECs. We next assessed the effect of EGFL7 on CPCs. CPCs were plated on fibronectin- or EGFL7-coated plates and cell numbers evaluated after 48 hours. Culture on EGFL7-coated plates resulted in significantly increased numbers of viable cells; this effect of EGFL7 was reversed by the addition of anti-EGFL7 (Figure 7D).

Given the preferential expression of *Egfl7* in CPCs, we next determined whether inhibition of EGFL7 in vivo alters the enumeration of these cells, thus constituting a potential circulating PD biomarker of anti-EGFL7 activity. To address this question, we evaluated the effect of anti-EGFL7 on CPCs in 2 preclinical models: the *RIP-TβAg* GEMM and the MDA-MB231 breast cancer xenograft model, where treatment with anti-EGFL7 (h18F7) in combination with murine anti-VEGF resulted in enhanced tumor growth inhibition compared with anti-VEGF alone (data not shown). In both instances, m18F7 and/or h18F7 was dosed for

Table 1
Anti-EGFL7 improves the durability of the antitumor response rate provided by anti-VEGF in a dose-dependent manner in the *Kras^{G12D};p53$^{Frt/Frt}$* NSCLC GEMM

	2 weeks		4 weeks		6 weeks	
Treatment	**% PR+StD[A]**	**% PD[A]**	**% PR+StD[A]**	**% PD[A]**	**% PR+StD[A]**	**% PD[A]**
C	58	42	11	89	0	100
V (5 mpk)	94	6	88	13	63	38
VE (5 + 0.1 mpk)	95	5	90	10	40	60
VE (5 + 1.0 mpk)	100	0	84	16	79	21
VE (5 + 25 mpk)	97	3	87	13	50	50

Quantitation of tumor burden response rates at approximately 2, 4, and 6 weeks after the start of the study. Tumor burden responses at each time point, all relative to the initial baseline micro-CT results, were classified as follows: PR if there was a greater than 30% reduction; StD if the percentage change was between –30% and 100%; PD if there was a greater than 100% increase. [A]Since very few PRs were observed, the number of PRs and StDs were pooled; the final PD percentage represents pooled numbers of PD and deaths (see Supplemental Figure 5 and Methods). The mice were dosed i.p. 2 times per week with control anti-ragweed IgG2a (5 mpk + 1.0 mpk), anti-VEGF (B20-4.1.1; 5 mpk), or a combination of anti-VEGF (5 mpk) plus anti-EGFL7 (m18F7) at 0.1, 1.0, or 25 mpk (see Figure 5). The VE (5 + 1.0 mpk) combination treatment cohort provided the most durable antitumor response rate.

2 weeks, after which FACS analysis was performed for enumeration of both CPCs and CECs. Similar to human peripheral blood, tumor-bearing animals exhibited both the CEC and CPC populations (Supplemental Figure 7D). Treatment with anti-EGFL7 resulted in a reduction in the number of CPCs compared with the control IgG and anti-VEGF groups in both models tested (Figure 7, E and F), occurring even at low doses of anti-EGFL7 in combination with anti-VEGF (Supplemental Figure 7E). Additionally, this effect was limited to CPCs, as CEC enumeration remained unaltered (data not shown).

Based on the preclinical observations, we included CPC evaluation as a potential PD biomarker of target inhibition in the phase I clinical study examining the humanized anti-EGFL7 antibody (h18F7, also called MEGF0444A). A phase Ia dose-escalation study examined single-agent h18F7 administered i.v. once every 3 weeks (q3wk). A second, phase Ib, study consisted of 2 arms: arm A examined escalating doses of h18F7 with a fixed dose of 10 mpk bevacizumab administered every 2 weeks (q2wk); arm B was similar to arm A except with the addition of paclitaxel (90 mg/m^2 every week, qwk) (Supplemental Figure 8). These studies were designed to assess the safety and pharmacokinetic (PK) properties of h18F7 as a single agent as well as in combination with bevacizumab and chemotherapy. Blood collections were performed at various early and late time points after administration of the first dose of drug for the enumeration of CPCs (see Supplemental Figure 8). Biomarker evaluation was not performed in the paclitaxel-containing arm of the phase Ib trial, as paclitaxel is known to mobilize peripheral blood progenitor cells (22), thus confounding the measurement of the effect of anti-EGFL7.

Prior to implementing the real-time assay in the clinic, assay characterizations were performed in whole blood from healthy donors to assess the intrasubject biological variability of the assay through the course of a 4-week period (Supplemental Figure 9A). In addition, each patient included in the phase I trials provided a double-baseline blood draw (approximately 1 week apart), which was used to estimate inherent biological variability within each patient (Supplemental Figure 9B). These data from healthy donors and the phase I population showed approximately 10% biological variability in the assay. A 30% deviation from the predose time point was thus considered a significant change, as it reflects a change in CPCs that is approximately 3 SDs away from the inherent biological variability. The prevalence of CPCs in humans is approximately 200–1000 cells/ml, and greater biological variability was observed in donors whose baseline levels were lower than 400 cells/ml. Thus, we applied a baseline threshold of 400 cells/ml for the analysis of patients in the phase I studies. Using these criteria, a reduction in CPCs was observed in the single-agent phase Ia study, in which approximately 50% of the patients in the 1 and 3 mpk cohorts showed a delayed and transient 30%–60% reduction in CPCs compared with their predose values (Figure 8A). In arm A of the phase Ib study, a dose-dependent change was observed: in the 5 mpk cohort, 4 of the 6 patients evaluated (67%) showed a 40%–60% reduction in CPCs, which was sustained through at least the first 2 cycles of dosing (Figure 8, B and C). We did not observe a correlation between either baseline CPC numbers or changes in CPCs and tumor volume changes measured by response evaluation criteria in solid tumors (RECIST) (data not shown).

Discussion

In the past decade, VEGF inhibitors have provided well-recognized clinical benefits to patients suffering from a number of solid cancers. The impetus to improve the efficacy of these agents has resulted in a better understanding of how VEGF inhibitors function. One important finding is that prolonged usage of the anti-VEGF antibody bevacizumab, either as a single agent or in combination with chemotherapy, resulted in greater benefit relative to shorter-term treatment (16, 23, 24). To maximally harness the potential of long-term VEGF inhibition as well as minimize side effects, we searched for targeted agents that could enhance anti-VEGF activity and identified anti-EGFL7 as one potential candidate.

Table 2
Superior tumor burden response rates observed with long-term anti-VEGF plus anti-EGFL7 treatment in the *Kras^{G12D};p53$^{Frt/Frt}$* NSCLC GEMM

	2 weeks		4 weeks		6 weeks	
Treatment	**% PR+StD**	**% PD**	**% PR+StD**	**% PD**	**% PR+StD**	**%PD**
VE	93	7	85	15	67[A]	33[A]
V2E2	89	11	64	36	18	82

Quantitation of tumor burden response rates at approximately 2, 4, and 6 weeks after the start of the study. Response rates were calculated and presented as previously defined (see Table 1, Supplemental Figure 6, and Methods). All mice were dosed i.p. with anti-VEGF (B20-4.1.1; 5 mpk) + anti-EGFL7 (m18F7; 1.0 mpk). VE = 2×/wk until the end of study; V2E2 = 2×/wk for 2 weeks only and then discontinued. The VE treatment cohort resulted in a significant change in response rates relative to V2E2 at the 6-week treatment interval. [A]$P = 3.91 \times 10^{-5}$.

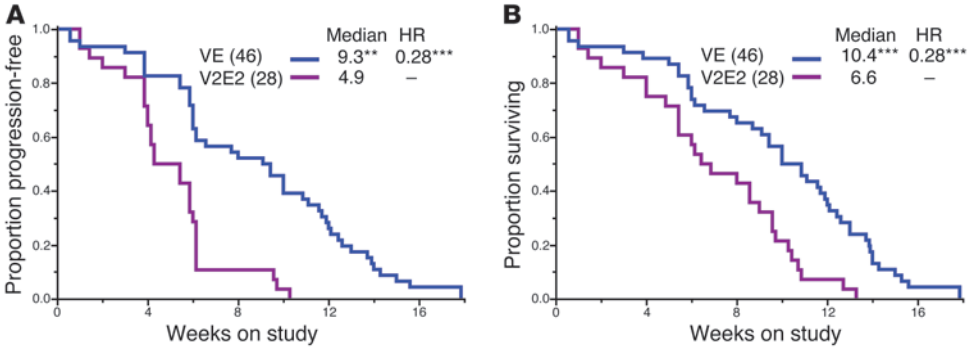

Figure 6

Superior efficacy observed with long-term anti-VEGF plus anti-EGFL7 treatment in the *Kras*^{G12D};*p53*$^{Frt/Frt}$ NSCLC GEMM. (**A** and **B**) Kaplan-Meier plots depicting PFS (**A**) and OS (**B**) rates. The number of mice per cohort is listed in parentheses. Median survival (in weeks) and HRs relative to V2E2 are shown. The VE treatment cohort provided significantly improved PFS and OS rates relative to V2E2, as determined by both log-rank and Cox-proportional hazard analyses. $^{**}P < 0.005$; $^{***}P < 0.0005$. For **A** and **B**, all antibodies were dosed i.p. with anti-VEGF (B20-4.1.1; 5 mpk) plus anti-EGFL7 (m18F7; 1.0 mpk). VE = 2 times per week until the end of the study; V2E2 = 2 times per week for 2 weeks only and then discontinued. The VE cohort is the same as shown in Figure 5, D and E.

Historically, several factors may have contributed to the low approval rate for novel oncology drugs. One is the predominant reliance on preclinical systems that fail to adequately mimic the tumor or its microenvironment: xenografts of human cancer cell lines or tumor explants in immunodeficient mice have been the primary in vivo model systems employed to interrogate therapeutic responsiveness (25, 26), despite their inability to reliably reflect observed human patient responses and predict overall outcomes (27, 28). A second factor affecting clinical trial success rates is the incorporation of biomarkers to inform patient selection and therapeutic activity, which has only become more routine over the past decade. Therefore, identification of more predictive and of more prognostic preclinical models and biomarkers are 2 important unmet needs necessary for the development of more effective anticancer therapies. Over the past decade, the increased repertoire and application of GEMMs of cancer that more faithfully recapitulate many aspects of their corresponding human disease have resulted in a renewed enthusiasm that they might better inform not only target validity and drug efficacy, but also aid in identifying optimal dosing regimens and PD biomarkers. The importance of this as well as their validity have recently been demonstrated in studies that examined therapeutic responses in both a retrospective and a prospective manner (15, 29). Moreover, GEMMs have been newly leveraged to conduct "coclinical" trials that are designed to mirror ongoing human clinical trials and identify predictive genetic and PD biomarkers that can be validated by interrogating patient samples collected from the concurrent human clinical trials (30).

In light of the above, we sought to interrogate the effect of dual EGFL7 and VEGF inhibition in preclinical model systems that more faithfully reflect the autochthonous microenvironment in which both angiogenic factors exert their primary action. We examined the in vivo efficacy of combined anti-EGFL7 and anti-VEGF using GEMMs as well as traditional xenografts of human cancer cell lines in immunodeficient mice. We demonstrate that this combination markedly delayed tumor growth, resulting in significant improvements in both PFS (log-rank, $P = 0.0147$; HR = 0.56, $P = 0.0412$) and OS (log-rank, $P = 0.0152$; HR = 0.51, $P = 0.0078$) benefits relative to single-agent anti-VEGF in a GEMM of NSCLC. Importantly, the magnitude of these effects reflects that which is often observed clinically. In addition, we found that relatively low doses of anti-EGFL7 were sufficient for maximal efficacy when used in combination with anti-VEGF. Interestingly, this observed dosage effect was consistently revealed only in the autochthonous GEMMs and not in subcutaneous xenograft models, suggesting the importance of interrogating these agents in their innate microenvironment.

We also evaluated the dose-drug activity relationship in the phase Ia and phase Ib clinical trials evaluating anti-EGFL7. We identified and developed a surrogate PD biomarker using a population of CD34$^+$ CPCs that responded to anti-EGFL7 treatment in preclinical models. While the ex vivo functional studies conducted suggest that these cells are capable of differentiating into ECs and exhibit gene expression profiles similar to progenitor cells, it is presently unclear whether these CPCs are hematopoietic progenitor cells. Gratifyingly, the PD response to anti-EGFL7 in human patients showed a remarkably similar dose dependency to that observed in GEMMs.

h18F7 in combination with bevacizumab does not exacerbate the safety profile of bevacizumab administered either as a doublet or in combination with chemotherapy (31). Hence, we were unable to identify a maximal tolerated dose (MTD) for this drug in combination with bevacizumab. Importantly, the phase I studies examining anti-EGFL7, both alone and in combination with bevacizumab, did not show signs of thrombocytopenia, neutropenia, or anemia, with some patients being on therapy for over 1 year (31). However, the phase II studies will be more informative for assessing the long-term safety profile. Based on the efficacy profile of anti-EGFL7 in preclinical models, single-agent clinical activity was not expected. With respect to clinical responses in the phase Ib combination study, 1 ovarian cancer patient demonstrated a RECIST grade PR at the 2 mpk level of arm B, 5 patients demonstrated PRs at the 5 mpk dose level in both arm A and B, and 1 head and neck cancer patient demonstrated a PR at the 10 mpk cohort of arm A (31). Since h18F7 was administered in combination with bevacizumab and chemotherapy, attributing these responses to the combination or the single agents is challenging. Given that PD biomarker modulation was observed in 67% of the patients at the 5 mpk, q2wk dose and clinical activity as measured by RECIST response criteria was observed at this dose, we chose 5 mpk, q2wk, or 7.5 mpk, q3wk, as the recommended phase II dose for h18F7 in combination with bevacizumab. The PK properties of h18F7 are consistent with typical IgG1 demonstrating linear PK with a terminal half-life of approximately 15 days (32), and PK modeling indicates that the doses at which PD activity was observed in humans had comparable exposures to the optimally efficacious doses in the GEMMs.

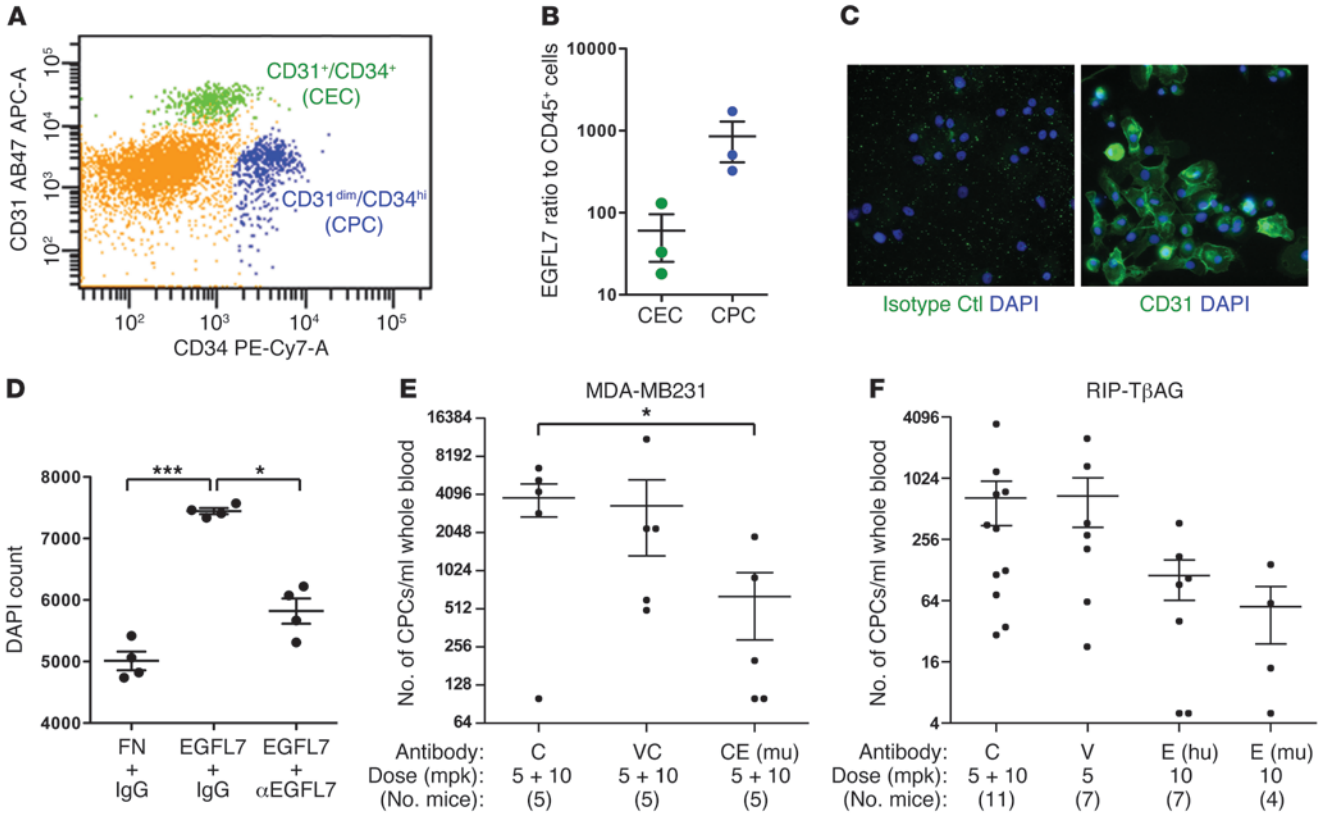

Figure 7

CPCs express EGFL7 and serve as a biomarker of anti-EGFL7 activity. (**A**) FACS-based expression of CD34 and CD31 was assessed in $CD45^{dim}$ cell population from human peripheral blood. Two distinct clusters of CEC (green) and CPC populations (blue) are shown. (**B**) Peripheral blood CECs, CPCs, and $CD45^+$ cells were sorted from 3 donors and evaluated for EGFL7 transcripts. The mean ± SEM is depicted. (**C**) CPCs (2×10^5/well) were allowed to differentiate on fibronectin-coated plates for 21 days. Cells were fixed and incubated with anti-CD31 or isotype control and cell nuclei stained with DAPI. Original magnification, ×40. (**D**) CPCs were plated in quadruplicate on either fibronectin- or EGFL7-coated plates (3×10^4/well). Cells were then treated with either control IgG or h18F7 and proliferation assessed by counting the number of $DAPI^+$ cells 48 hours later. The mean ± SD is depicted ($n = 4$ biological replicates). $^*P < 0.05$; $^{***}P < 0.0001$. (**E**) Mice bearing MDA-MB231 xenografted tumors were treated with control anti-ragweed plus anti-gD, anti-VEGF plus control anti-gD, or control anti-ragweed plus anti-EGFL7 (mu; m18F7). Antibodies were dosed i.p. either 2 times per week (anti-ragweed and anti-VEGF) or 1 time per week (anti-gD and anti-EGFL7). (**F**) *RIP-TβAg* mice were treated with control anti-ragweed plus anti-gD, anti-VEGF, anti-EGFL7 (hu; h18F7), or anti-EGFL7 (mu; m18F7). Antibodies were dosed i.p., 1 time per week on days 1 and 8. (**E** and **F**) Whole blood was collected on day 19 (**E**) or 15 (**F**) for CPC enumeration. The mean ± SEM is depicted.

Historically, most marketed oncology drugs are dosed at their MTD, despite a clear lack of sufficient clinical evidence demonstrating activity equivalence to maximal efficacious dose (MED). Here, we integrated GEMMs and a clinical PD biomarker in cancer patients to inform a large molecule drug development program. This approach revealed clear dose-dependent activities of a novel antiangiogenic agent, anti-EGFL7, both preclinically and clinically, thereby underscoring the utility of GEMMs and biomarkers in guiding clinical trial design, including dose selection. Importantly, this study offers a potential novel therapeutic agent, anti-EGFL7, to treat solid tumors and provides a promising alternative for cancer patients.

Methods

Antibodies and proteins. Recombinant EGFL7 proteins and anti-EGFL7 antibodies were generated as previously described (10). Antibody characterization and reformatting is described in the Supplemental Methods.

HUVEC caspase-3 and caspase-7 assays. Wells of Maxisorb 96-well plates (#456537; Nunc) were coated overnight with the following: carbonate buffer (pH 9.6), 0.1 mg/ml poly-lysine (P4707; Sigma-Aldrich) 2 μg/ml fibronectin (#11051407001; Roche), 5 μg/ml osteopontin (14433-PO; R&D Systems), 5 μg/ml EGFL7 (Genentech; ref. 10), or fibronectin plus EGFL7 in carbonate coating buffer (pH 9.6). After 1 PBS wash, 20,000 HUVEC (Lonza) per well was added in EGM-2 medium (Lonza) and cells were left to adhere for 4 hours in the tissue culture incubator. Medium was then replaced with either fresh EGM-2, EGM-2 with 400 μM deferoxamine mesylate salt (DFX) (D9533; Sigma-Aldrich), EGM-2 with 200 μM cobalt chloride ($CoCl_2$) (#C2644; Sigma-Aldrich), or EGM-2 (Lonza) with and without 10 μg/ml anti-EGFL7 antibody (GNE). Cells were cultured under these conditions overnight. Cleaved caspase-3 and caspase-7 activity was assayed using the Caspase-Glo 3/7 Assay Kit (# G8091; Promega), and cell numbers in each well were measured using CyQuant (C7026; Molecular Probes) according to the manufacturer's instructions. In experiments with $CoCl_2$, cell numbers were not measured at study end point due to color interference by $CoCl_2$. In all other experiments, the levels of apoptosis were expressed as the ratio of caspase-3 and caspase-7 activity versus cell number. Each experiment was repeated at least 3 times, and results were similar. Representative experiments are presented in Figure 1.

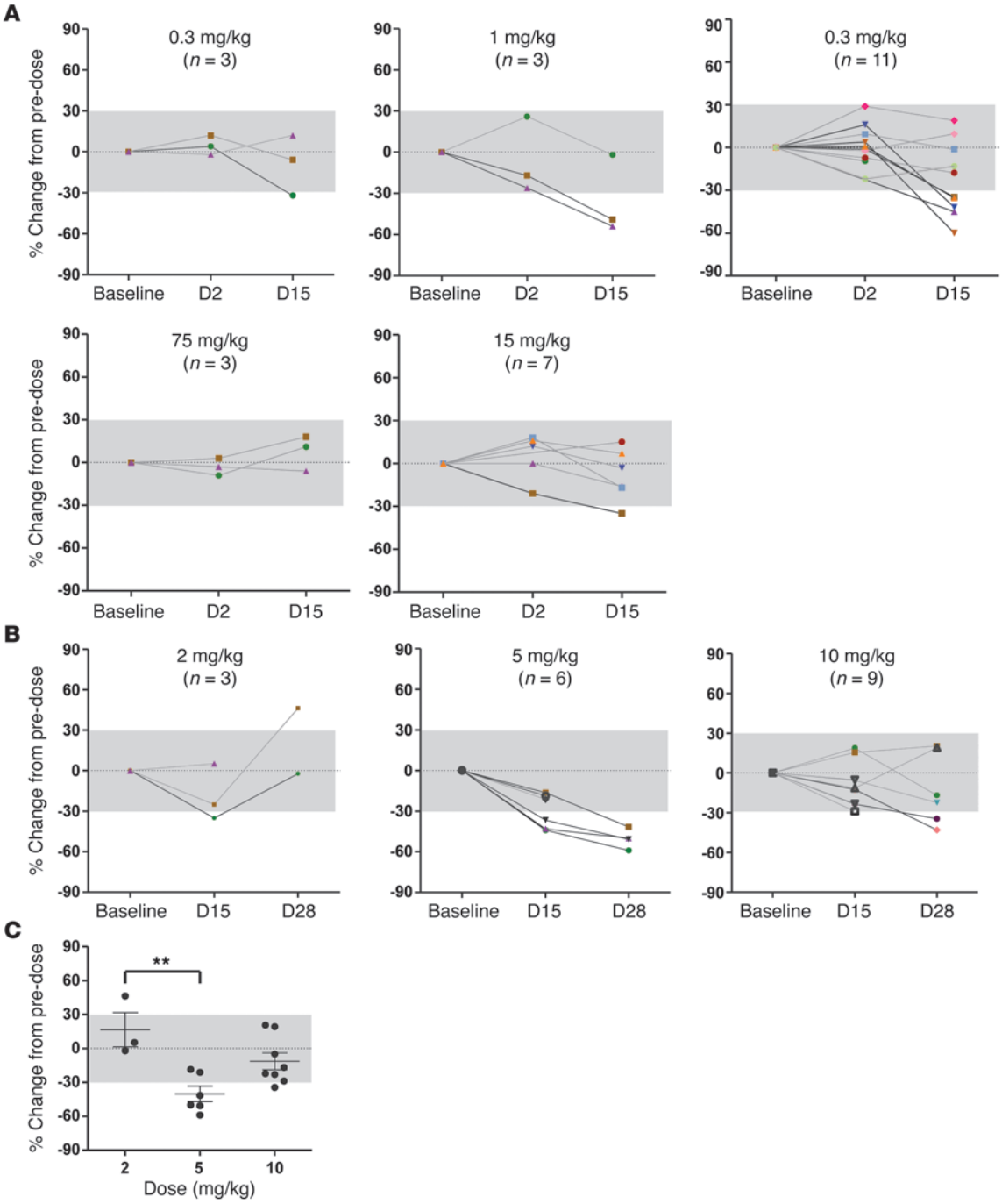

Figure 8

Evaluation of CPCs in phase I studies for anti-EGFL7. (**A**) Enumeration of CPCs in a phase Ia study with single agent MEGF0444A. Whole blood was collected at screen, predose, and at days 2 and 15 after infusion of MEGF0444A from all patients in the phase Ia study. Increasing doses of MEGF0444A were administered i.v. once every 3 weeks. Blood was shipped overnight for enumeration of absolute counts of CPCs by flow cytometry. The *y* axis represents the percentage change from baseline (average of screen and predose) values. (**B**) Enumeration of CPCs in a phase Ib study with MEGF044A and bevacizumab. Increasing doses of MEGF0444A were administered with a fixed dose of 10 mpk bevacizumab once every 2 weeks. Whole blood was collected at screen, predose, and at days 2, 15, and 28 after first infusion of MEGF0444A and bevacizumab from all patients in the phase Ib study. Blood was shipped overnight for enumeration of absolute counts of CPCs by flow cytometry. The *y* axis represents percentage change from baseline (average of screen and predose) values. (**C**) Representative change in CPCs at day 15 or 28 for patients in the 3 dose groups of MEGF0444A from the phase Ib trial. $^{**}P < 0.001$

GEMMs. The *RIP-TβAg* and *Kras^{G12D}; p53$^{Frt/Frt}$* NSCLC GEMMs were generated as previously described (15, 21) and maintained on a C57BL/6J-Tyr strain background. *RIP-TβAg* mice were provided a high-sugar diet as well as 10% sucrose in their drinking water to alleviate tumor-associated hyperinsulinemia.

Animal treatment regimens and monitoring. Anti-VEGF antibodies (B20-4.1 or B20-4.1.1; both are mouse IgG2a), anti-EGFL7 antibodies (m18F7, mouse IgG2b; h18F7, human IgG1), and control antibodies (anti-ragweed, mouse IgG2a; anti-gD, human IgG1) were prepared and purified at Genentech Inc. All antibody lots were quality controlled to ensure low endotoxin levels; routine levels run at approximately 0.01 endotoxin units (EU)/mg, with a maximum cutoff of less than 0.5 EU/mg. All chosen dosing regimens were well tolerated.

RIP-TβAg transgenic tumor-bearing mice at 11–12 weeks of age were randomized into various treatment groups. All antibodies were dosed via i.p. injection once weekly for 2 weeks on days 1 and 8. Control group received anti-ragweed (murine IgG2a) at 5 mpk + anti-gD (human IgG1) at 10 mpk; anti-VEGF group received B20-4.1.1 (murine IgG2a) at 5 mpk; anti-EGFL7 received m18F7 (murine IgG2b) at 10 mpk; anti-EGFL7 received h18F7 (human IgG1) at 10 mpk; combination groups received anti-VEGF (B20-4.1.1) at 5 mpk + anti-EGFL7 (h18F7) at 0.3, 1.5, 10, or 50 mpk. Histological analysis and tumor MVD quantification of tumors from the *RIP-TβAg* transgenic mice are described in the Supplemental Methods.

Kras^{G12D};p53$^{Frt/Frt}$ mice were infected at 7–9 weeks of age with 5×10^6 infectious units of Adeno-FLPe/IRES/CRE as previously described (15). Mice were imaged at 16 weeks after infection via x-ray micro-CT (15, 21). The calculated tumor burden, body weight, and sex were used to randomize mice into treatment cohorts. Antibodies were dosed via i.p. injection twice weekly until the end of the study for long-term survival studies. Control group received anti-ragweed at 5 mpk plus anti-ragweed at 1.0 mpk; anti-VEGF group received B20-4.1.1 at 5 mpk; anti-EGFL7 group received murine MAb 18F7 (m18F7) at 1 mpk; combination groups received B20-4.1.1 at 5 mpk + m18F7 at 0.1, 1.0, or 25 mpk. Animals received serial micro-CT scans at 4 weeks or 2, 4, and 6 weeks after the start of the study (Tables 1 and 2, Figures 5 and 6, and Supplemental Figures 5 and 6). Note that the median OS curve reported here for the anti-VEGF cohort shown in Figure 5, C, E, and G, increased from 8.1 weeks (as reported in ref. 21) to 8.4 weeks, as a newer version of JMP (version 9.0) was used to generate the Kaplan-Meier survival curves and calculate median OS values for the cohorts being grouped and analyzed herein; the algorithm JMP 9.0 uses to calculate median OS values changed relative to that in earlier software versions.

For cell-transplant studies, cultured tumor cells were resuspended in PBS and implanted subcutaneously at a concentration of 1×10^7 cells (MDA-MB231 and H1299) into the right flank of HRLN *nu/nu* mice. Mice with mean tumor volumes of 80–200 mm^3 (MDA-MB231) or 75–150 mm^3 (H1299) were grouped into treatment cohorts of 5–12 mice each, respectively. Treatment groups included anti-ragweed control, murine anti-VEGF antibodies (B20-4.1 or B20-4.1.1), or anti-EGFL7 antibodies (m18F7 or h18F7) administered i.p. in PBS; doses and regimens are indicated in figure legends. For the PD studies, whole blood was collected via cardiac puncture and stored on ice for FACS analysis.

All animals were dosed and monitored according to guidelines from the Institutional Animal Care and Use Committee (IACUC) at Genentech Inc. Accordingly, animals were monitored daily and body weights measured at least twice weekly. For the xenograft studies, tumors and body weights were measured twice weekly, and mice were taken off the study when their tumors reached 1000 mm^3 (H1299 model). Animals were censored for survival based either on mortality or predetermined morbidity criteria for euthanasia (in consultation with the veterinary staff), which included hunching, ruffled fur, belabored breathing, low body temperature, lack of mobility, and/or a greater than 20% body weight loss from the time of the start of the study.

Preclinical trial endpoints for Kras^{G12D};p53$^{Frt/Frt}$ NSCLC GEMM. We measured PFS and OS as previously reported (15). To account for the rapid growth of mouse tumors, we defined disease progression as a doubling in tumor burden and used that criterion to build PFS Kaplan-Meier curves. Tumor burden responses were determined at 2, 4, and 6 weeks after first treatment dose, all relative to the initial baseline micro-CT result, and were classified as follows: PR if there was a greater than 30% reduction; StD if the change was between –30% and 100%; progressive disease (PD) if there was a greater than 100% increase. Since very few PRs were observed, the number of PRs and StDs were pooled; the final PD percentage represents pooled numbers of PD and deaths.

Statistical analyses for Kras^{G12D}; p53$^{Frt/Frt}$ NSCLC GEMM. In Figures 5 and 6 showing Kaplan-Meier survival curve estimates, a Cox proportional hazards model was fit to the data in the R statistical language using the "survival" library as previously described (15). Briefly, study baseline tumor burden (logarithmically scaled, with 1 added to each scan's value to specify a baseline of 0 on the logarithmic scale), sex, and treatment group were included for each mouse as explanatory factors. The endpoint for mice was survival time (OS) or the minimum of survival and time to doubling in tumor size (PFS). We defined "time to progression" as the first time that a scan yielded a value double the value of the smallest scan recorded regardless of when that value was recorded. Ties in event times were resolved with Efron's approximation. All *P* values reported for hazard ratios (HRs) are 2 sided, and test the null hypothesis that the HR is 1 between the 2 groups specified; a *P* value of less than 0.05 related to the HR test indicated the HR between the 2 specified groups was significantly different. The Benjamini–Hochberg procedure (33) was applied to adjust the *P* values from the multiple comparisons.

The imaging plots in Supplemental Figure 5A and Supplemental Figure 6A show the tumor burdens versus time in study for control and select treatment cohorts over a period of 6 weeks. Each line represents the tumor burden for 1 animal, and the solid lines are the fitted lines from a linear mixed effect model (34), implemented with the "nlme" package in R (35). The linear mixed effect model had the fixed effect of treatment and a random intercept for each animal. The growth rate in tumor burden for each treatment was estimated as the slope of the longitudinal growth curve. Pair-wise differences in slopes across groups were evaluated by the contrasted slope estimates. The Tukey-Kramer method (36) was applied to correct for the multiple tests performed using the "multcomp" package in R. Fisher's exact test (37) was applied for response rate analyses in Tables 1 and 2 as well as Supplemental Figure 5B and Supplemental Figure 6B.

Flow cytometry for evaluation of CD34$^+$ cells in murine whole blood. Blood was collected into EDTA tubes via cardiac puncture on day 19 (MDA-MB231) or day 14 (*RIP-TβAg*) and analyzed for circulating CD34$^+$ cells using a Lyse No Wash flow cytometry assay protocol. Specifically, 100 μl of blood was stained in TruCount tubes for 30 minutes with the following panel: Syto16 (Invitrogen), CD31-PE (BD Biosciences), CD34-Alexa Fluor 647 (BD Biosciences), and CD45-PerCP-Cy5.5 (BD Biosciences). The stained blood was lysed/fixed for 10 minutes with 500 μl BD FACSLyse, 500 μl PBS was added to the sample, and the stained cells were acquired on the BD FACSCanto cytometer. Data were analyzed on FACSDiva, and absolute cell counts were determined using the TruCount quantitation method. CD45^{dim}CD31^{dim} CD34^{hi} cells were classified as CPCs and CD45^{dim}CD31$^+$CD34$^+$ cells were classified as CECs.

A series of analyses were performed to determine the relationship between baseline CPC counts and our ability to measure significant changes. We found that average baseline CPC counts below 400 cells/ml seriously compromised our ability to determine treatment effect. There-

fore, we set 400 CPCs/ml as a cutoff to determine which models could be used to evaluate CPC response to treatment. The average baseline CPC counts were 3840 cells/ml and 655 cells/ml for the MDA-MB231 xenograft and *RIP-TβAg* models, respectively. The baseline mean CPC count in the mutant *Kras;p53*-driven NSCLC model was 354 cells/ml; thus we are unable to reliably measure CPCs in this model.

Flow cytometry for evaluation of CD34⁺ cells in human whole blood. The phase Ia (clinicaltrials.gov identifier NCT00909740; MEF4693g) and phase Ib studies (clinicaltrials.gov identifier NCT01075464; MEF4797g) consisted of dose-escalating studies in patients with advanced solid tumors to evaluate the safety and PK profiles of MEGF0444A either alone or in combination with bevacizumab, respectively. All patients in the trials provided written informed consent for use of tissues and biofluids for exploratory analysis of biomarkers.

Patient blood was collected into EDTA tubes and analyzed for $CD34^+$ cells using a protocol similar to that used for the mouse assay, but with the following panel: Syto16 (Invitrogen), CD31 PE-Cy7, CD34-APC, CD45 APC-Cy7, and CD133 PE (all from BD Biosciences). As before, absolute counts of CPCs were calculated using the TruCount quantitation method. CPC acquisition for the phase Ib study was performed at Esoterix and analyzed at Genentech Inc.

Purification and analysis of CD34⁺ cells from human whole blood. PBMCs were purified using Ficoll gradient from EDTA blood collected from healthy adult volunteers. $CD45^+$ (PBMC), $CD45^{Dim}CD31^+CD34^+$ (CEC), and $CD45^{dim}CD31^{dim}CD34^{hi}$ (CPC) were sorted on FACSAria. RNA was extracted from the cells using the Arcturus PicoPure RNA Extraction Kit (Life Technologies Corp.) following the protocol supplied by the manufacturer. For each sample, a 2-round amplification process for RNA was performed using TargetAmp 2-Round Biotin-aRNA Amplification Kit 3.0 (Epicentre Biotechnologies). Expression of EGFL7 transcript in each of the sorted populations was assessed by TaqMan qPCR.

Statistics. Unless otherwise specified in individual cases, statistical analyses were performed using unpaired, 2-tailed Student's *t* test, and *P* values were calculated using Graphpad Prism software. Pair-wise comparisons with *P* values equal to or less than 0.05 were deemed statistically significant.

Study approval. All animal studies were reviewed and approved by the IACUC at Genentech Inc. The phase I study was reviewed and approved by the human ethics committees of Pinnacle Oncology and Hematology (Scottsdale, Arizona, USA), UCSF Helen Diller Family CCC (San Francisco, California, USA), and Premier Oncology (Santa Monica, California, USA). All patients who participated in this phase I study provided written, informed consent.

Acknowledgments

We thank Ina Rhee for her thoughtful and constructive comments regarding the manuscript. We are very grateful to Patricia Hamilton, Jason Long, Ely Cosino, Janeko Bower, Vincent Javinal, Alfonso Arrazate, Rebecca Hong, Lee Nguyen, Tiffany Yuan, and Alfred Wong for providing excellent technical assistance to support the GEMM preclinical studies and evaluation as well as Shang-fan Yu, Sarajane Ross, and Stephen Gould for supporting the xenograft studies. Jean-Philippe Stephan, Yu-Ju Meng, Pamela Chan, Jo-Anne Hongo, Kurt Schroeder, Shuang Bai, Eric Wakshull, Leon H. Parker, Kristin Bowles, and Dan Eaton made substantial contributions to the characterization of the anti-EGFL7 antibodies. Hok Seon Kim, Racquel Corpuz, Richard Vandlen, and Dan Yansura generated the recombinant EGFL7 proteins. We are indebted to Suzanne van Dijk for her excellent preparation of tumor tissues for electron microscopy. We also received extensive and invaluable technical support from the protein chemistry, antibody engineering, and pathology departments as well as the genotyping and murine reproductive technology core labs. We thank Oded Foreman for providing IHC images. We would also like to thank Michelle Schweiger for in vivo study support and Junko Aimi and Heejo Baek for clinical sample operations support.

Received for publication November 19, 2012, and accepted in revised form June 13, 2013.

Address correspondence to: Leisa Johnson, Genentech Inc., 1 DNA Way, Rm 12-322, MS 37, South San Francisco, California 94080, USA. Phone: 650.467.7381; Fax: 650.225.6412; E-mail: johnson.leisa@gene.com. Or to: Weilan Ye, Genentech, Inc., 1 DNA Way, Rm 13-3077, MS 93b, South San Francisco, California 94080, USA. Phone: 650.225.4448; Fax: 650.467.7571; E-mail: ye.weilan@gene.com. Or to: Priti Hegde, Genentech, Inc., 1 DNA Way, Rm 42-2180, MS 422a, South San Francisco, California 94080, USA. Phone: 650.225.6145; Fax: 650.225.1998; E-mail: hegde.priti@gene.com.

1. Jayson GC, Hicklin DJ, Ellis LM. Antiangiogenic therapy-evolving view based on clinical trial results. *Nat Rev Clin Oncol*. 2012;9(5):297–303.
2. Ferrara N, Gerber HP, LeCouter J. The biology of VEGF and its receptors. *Nat Med*. 2003;9(6):669–676.
3. Benjamin LE, Keshet E. Conditional switching of vascular endothelial growth factor (VEGF) expression in tumors: induction of endothelial cell shedding and regression of hemangioblastoma-like vessels by VEGF withdrawal. *Proc Natl Acad Sci U S A*. 1997;94(16):8761–8766.
4. Inai T, et al. Inhibition of vascular endothelial growth factor (VEGF) signaling in cancer causes loss of endothelial fenestrations, regression of tumor vessels, and appearance of basement membrane ghosts. *Am J Pathol*. 2004;165(1):35–52.
5. Willett CG, et al. Direct evidence that the VEGF-specific antibody bevacizumab has antivascular effects in human rectal cancer. *Nat Med*. 2004;10(2):145–147.
6. O'Connor JP, et al. Quantifying antivascular effects of monoclonal antibodies to vascular endothelial growth factor: insights from imaging. *Clin Cancer Res*. 2009;15(21):6674–6682.
7. Campagnolo L, et al. EGFL7 is a chemoattractant for endothelial cells and is up-regulated in angiogenesis and arterial injury. *Am J Pathol*. 2005;167(1):275–284.
8. Fitch MJ, Campagnolo L, Kuhnert F, Stuhlmann H. Egfl7, a novel epidermal growth factor-domain gene expressed in endothelial cells. *Dev Dyn*. 2004; 230(2):316–324.
9. Soncin F, et al. VE-statin, an endothelial repressor of smooth muscle cell migration. *EMBO J*. 2003; 22(21):5700–5711.
10. Parker LH, et al. The endothelial-cell-derived secreted factor Egfl7 regulates vascular tube formation. *Nature*. 2004;428(6984):754–758.
11. Huang CH, Li XJ, Zhou YZ, Luo Y, Li C, Yuan XR. Expression and clinical significance of EGFL7 in malignant glioma. *J Cancer Res Clin Oncol*. 2010; 136(11):1737–1743.
12. Schmidt M, et al. EGFL7 regulates the collective migration of endothelial cells by restricting their spatial distribution. *Development*. 2007; 134(16):2913–2923.
13. Xu D, Perez RE, Ekekezie, II, Navarro A, Truog WE. Epidermal growth factor-like domain 7 protects endothelial cells from hyperoxia-induced cell death. *Am J Physiol Lung Cell Mol Physiol*. 2008; 294(1):L17–L23.
14. Nichol D, et al. Impaired angiogenesis and altered Notch signaling in mice overexpressing endothelial Egfl7. *Blood*. 2010;116(26):6133–6143.
15. Singh M, et al. Assessing therapeutic responses in Kras mutant cancers using genetically engineered mouse models. *Nat Biotechnol*. 2010;28(6):585–593.
16. Burger RA, et al. Incorporation of bevacizumab in the primary treatment of ovarian cancer. *N Engl J Med*. 2011;365(26):2473–2483.
17. Takimoto CH. Maximum tolerated dose: clinical endpoint for a bygone era? *Target Oncol*. 2009; 4(2):143–147.
18. Hurwitz HI, Yi J, Ince W, Novotny WF, Rosen O. The clinical benefit of bevacizumab in metastatic colorectal cancer is independent of K-ras mutation status: analysis of a phase III study of bevacizumab with chemotherapy in previously untreated metastatic colorectal cancer. *Oncologist*. 2009;14(1):22–28.
19. Shojaei F, Singh M, Thompson JD, Ferrara N. Role of Bv8 in neutrophil-dependent angiogenesis in a transgenic model of cancer progression. *Proc Natl Acad Sci U S A*. 2008;105(7):2640–2645.
20. Inoue M, Hager JH, Ferrara N, Gerber HP, Hanahan D. VEGF-A has a critical, nonredundant role in angiogenic switching and pancreatic beta cell carcinogenesis. *Cancer Cell*. 2002;1(2):193–202.
21. Singh M, et al. Anti-VEGF antibody therapy does not promote metastasis in genetically engineered mouse

tumour models. *J Pathol*. 2012;227(4):417–430.
22. Burtness BA, et al. A phase I study of paclitaxel for mobilization of peripheral blood progenitor cells. *Bone Marrow Transplant*. 1999;23(4):311–315.
23. Grothey A, et al. Bevacizumab beyond first progression is associated with prolonged overall survival in metastatic colorectal cancer: results from a large observational cohort study (BRiTE). *J Clin Oncol*. 2008;26(33):5326–5334.
24. Giantonio BJ. Targeted therapies: Goldie-Coldman and bevacizumab beyond disease progression. *Nat Rev Clin Oncol*. 2009;6(6):311–312.
25. Sausville EA, Burger AM. Contributions of human tumor xenografts to anticancer drug development. *Cancer Res*. 2006;66(7):3351–3354.
26. Suggitt M, Bibby MC. 50 years of preclinical anticancer drug screening: empirical to target-driven approaches. *Clin Cancer Res*. 2005;11(3):971–981.
27. Frese KK, Tuveson DA. Maximizing mouse cancer models. *Nat Rev Cancer*. 2007;7(9):645–658.
28. Kerbel RS. Human tumor xenografts as predictive preclinical models for anticancer drug activity in humans: better than commonly perceived-but they can be improved. *Cancer Biol Ther*. 2003; 2(4 suppl 1):S134–S139.
29. Singh M, Murriel CL, Johnson L. Genetically engineered mouse models: closing the gap between preclinical data and trial outcomes. *Cancer Res*. 2012; 72(11):2695–2700.
30. Chen Z, et al. A murine lung cancer co-clinical trial identifies genetic modifiers of therapeutic response. *Nature*. 2012;483(7391):613–617.
31. Naumovski L, et al. A phase Ib dose-escalation study of the safety, pharmacokinetics (PK), pharmacodynamics (PD), and antitumor activity of the humanized monoclonal antibody (huMAb) anti-EGFL7 (MEGF0444A) in combination with bevacizumab with or without paclitaxel in patients with advanced solid tumors. *J Clin Oncol*. 2011; 29(suppl):abstr2514.
32. Xin Y, et al. Population pharmacokinetic (PK) analysis supports fixed dosing for the humanized monoclonal antibody (huMAb) anti-EGFL7 (MEGF0444A) administered intravenously in patients with advanced solid tumors. *J Clin Oncol*. 2011; 29(suppl):abstr2586.
33. Benjamini Y, Hochberg Y. Controlling the false discovery rate: a practical and powerful approach to multiple testing. *J R Stat Soc Series B Stat Methodol*. 1995;57(1):289–300.
34. Laird NM, Ware JH. Random-effects models for longitudinal data. *Biometrics*. 1982;38(4):963–974.
35. Pinheiro J, Bates D, DebRoy S, Sarkar D. *Linear and Nonlinear Mixed Eects Models*. Vienna, Austria: R Development Core Team, R package version 3.1-101; 2011.
36. Hsu JC. *Multiple Comparison*. London, United Kingdom: Chapman and Hall; 1996.
37. Fisher RA. On the interpretation of $\chi 2$ from contingency tables, and the calculation of P. *J R Stat Soc Series B Stat Methodol*. 1922;85(1):87–94.